Journal of Alloys and Compounds 646 (2015) 1036–1042

Contents lists available at ScienceDirect

Journal of Alloys and Compounds

journal homepage: http://www.elsevier.com/locate/jalcom

Letter

MAX phase Ti_2AlC foams using a leachable space-holder material

Keywords:
MAX phases
Ti_2AlC
Porous materials
Eco-friendly processing
Water-soluble space-holder

A B S T R A C T

MAX phase foams from commercial Ti_2AlC powder were prepared by a powder processing method using raw sugar as space-holder. Manufacturing MAX phase foams using this method involves mixing Ti_2AlC powder with raw sugar, pressing the mixture to form a green body followed by space-holder removal and sintering. Green bodies were formed using cold uniaxial pressing and porosity was controlled varying the size and amount of the raw sugar space-holder. Three different space-holder particles sizes in the range of 250–1000 μm and four different volume amounts (20%, 40%, 60% and 80%) of space-holder were studied. The foams produced were characterized, and the size distribution and amount of resulting porosity was compared with the theoretically expected values. Optimal conditions using this processing technique for this material were established aiming towards controlling the final microstructures and properties, of porous Ti_2AlC MAX phase.

1. Introduction

Ti_2AlC belongs to a group ternary compounds referred to as $M_{n+1}AX_n$ phases or MAX phases, where M is a transition metal, A is an IIA or IVA element and X is C or N, n = 1, 2 or 3 [1]. MAX phases, due to their nanolaminate structure, exhibit unique properties that combine characteristics common to metals such as good thermal and electrical conductivity, good machinability, and damage tolerance with ceramic properties such as high elastic modulus, thermal shock resistance, excellent corrosion/oxidation resistance and self-healing capabilities at high temperature [2,3]. Among the more than 70 MAX phases reported so far, Ti_2AlC is the most light-weight (density of 4.11 g/cm^3 [1]) and oxidation resistant [4–9], it has good thermal (46 W/mK [10]) and electrical (2.78 $\mu\Omega^{-1}$ m^{-1} [2]) conductivity making it a good candidate for many high-temperature applications such as gas burner nozzles, heating elements and high temperature electrodes [2].

So far the majority of studies reported on this material are on fully dense material. The unique characteristics of MAX phase materials make them ideal for high performance applications which require high efficiency and low weight components capable of working in extreme conditions such as diesel particle filters, heat exchangers, solar volumetric collectors, catalyst substrates and impact-resistant structures. For this kind of applications, porous micro and macrocellular structures become part of the original component design providing added value and high performance. However, only a few recent studies have focused on porous Ti_2AlC [11–19], including some studies on MAX phases/Mg composites fabricated by melt infiltration of porous MAX phase performs [20–22], with exceptional mechanical damping capabilities. In these studies the methods used have been: incomplete densification during sintering or reactive sintering [11–17,20,21], replica method using polyurethane foams [23], and the use of NaCl as space-holder [18,19]. Space-holder method produces open and closed porosity by addition of space-holder or pore former. The size and shape of the pores are controlled through the morphology characteristics of the space-holder and the amount of porosity is controlled by the metal/powder volume ratio [24]. Elimination of some space-holders is performed by heating at high temperature. This step can result in gas formation during sintering that can lead to cracks in the foam. Leachable space-holders, such as NaCl, permits easy elimination by dissolution in water before sintering and avoids gas formation during sintering. This method has been studied and good results have been reported for many alloys [25]. NaCl has been employed to make Ti_2AlC foams, however pore shape became elliptical and oriented, rather than the cubic–like shape of NaCl particles, as a consequence of deformation of the particles during cold pressing [18]. Foams have also been produced employing crystalline carbohydrate as a space-holder and soaking in water under controlled conditions before sintering [26–33], however, MAX phase foams have not been previously produced using this method. These studies have reported that employing sugar as space-holder the internal architecture of the foam is controlled as well as porosities and pore size.

Control of porosity allows tailoring of mechanical and functional properties, and several studies reveal that porous MAX phases have potential applications as: supports for highly efficient catalytic devices [23,34] or MAX phases/Mg composites for mechanical dumping [14,21,22]. Porous Ti_2AlC presents potential in applications as solar volumetric collector because of its combination of good corrosion and oxidation resistance and good mechanical properties at high temperature [1–3].

http://dx.doi.org/10.1016/j.jallcom.2015.05.235
0925-8388/

In this study a simple and inexpensive space-holder method for manufacturing Ti_2AlC foams is reported using crystalline carbohydrate (raw sugar) particles as a leachable agent. Weight measurements were performed to determine the extent of space-holder removal. The cell morphology and porosity of produced foams was characterized.

2. Materials and methods

Ti_2AlC powder was provided by Sandvik (Sweden). The powder's average particle size was characterized using a Mastersizer 2000 equipment (D_{50} = 9 μm), the specific surface area using BET (2.7674 m^2/g) and the density of the powder was determined using a helium pycnometer Accupyc (4.122 g/cm^3). The phase constitution of the powder and sintered material was determined by X-ray diffraction resulting in two major phases: Ti_2AlC (ICSD: 165460) and Ti_3AlC_2 (ICSD: 153266), and minor phases: Al_2O_3 (ICSD: 10425) and TiC (ICSD: 44495). The powder was mixed with 2% of acrowax C ($C_{38}H_{76}N_2O_2$) (Lonza) atomized lubricant to facilitate the pressing step. The space-holder used was commercial raw sugar, in three size distributions: 250–400 μm, 400–800 μm and 800–1000 μm that were obtained by sieving the raw sugar. The particle size distribution in each of the three ranges was measured after sieving using a Mastersizer 2000 equipment and is given in Table 1. The powder and the space-holder were mixed in a Turbula® mixer for 1 h. Four different volume percentages of space-holder were used: 20%, 40%, 60% and 80%. Blends were pressed in a uniaxial cylindrical die (16 mm in diameter) at 800 MPa obtaining the green body. The space-holder was dissolved prior to sintering by soaking in water, during 12 h at 60 °C. Then the samples were dried during 24 h at 30 °C. To control sugar elimination two verifications were performed: a) mass loss, where the green body mass was measured before and after space-holder dissolution and was compared to the expected mass loss for complete sugar removal, considering the vol % of space-holder added, and b) chemical analysis, using LECO-CS200 equipment, where the weight % of carbon present in the sintered foams was compared to the carbon content present in the powder prior to blending as well as to the carbon in the sintered samples without space-holder. Subsequently, the sintering was performed in vacuum (10^{-5} mbar) at 1400 °C during 4 h including a 30 min dwell at 400 °C for delubrication purposes. Shrinkage of the samples due to sintering was measured by standard dimension measurement of the samples prior and after sintering using calipers. Open, closed and total porosity of foams was estimated as specified by ASTM C20-00 applying the ethanol immersion method based on Archimedes' principle and using the following equations:

$$\rho = \frac{dry\ mass \cdot \rho_{ethanol}}{wet\ mass - suspended\ mass} \quad (1)$$

$$Porosity_{overall}(\%) = \left(1 - \frac{\rho}{\rho_{teorethical}}\right) \cdot 100 \quad (2)$$

$$Porosity_{open}(\%) = \left(\frac{wet\ mass - dry\ mass}{wet\ mass - suspended\ mass}\right) \cdot 100 \quad (3)$$

$$Porosity_{closed}(\%) = Porosity_{overall}(\%) - Porosity_{open}(\%) \quad (4)$$

Table 1
Space-holder size distribution for each space-holder size range.

Space-holder range (μm)	D_{10} (μm)	D_{50} (μm)	D_{90} (μm)
250–400	259	385	571
400–800	448	640	924
800–1000	696	1015	1466

where "dry mass" is the mass (in g) of the dry sample, "wet mass" is the mass of the sample after soaking in ethanol during 2 h, "suspended mass" is the mass of the sample suspended in ethanol using a suspending system, $\rho_{ethanol}$ is the density (g/cm^3) of ethanol, $Porosity_{overall}$ is the volume percentage of the overall porosity of the sample, $Porosity_{closed}$ is the volume percentage of the closed porosity of the sample and $Porosity_{open}$ is volume percentage of the open porosity of the sample. The theoretical density of the powder, $\rho_{theoretical}$, was determined measuring powder density with an Accupyc helium pycnometer.

The cell morphology of foams was characterized using a scanning electron microscope (SEM) (JEOL-6500F). Metallographic preparation included grinding with SiC abrasive paper and polishing with 1 micron diamond powder. Image analysis was performed by image-J software on SEM images of foams with three different size distributions and the same amount of space-holder (60 vol.%). Each foam was analyzed using SEM images which where representative of the porosity of the sample. The images were binarized to define pore area and pore size. The average pore size and standard deviation were determined by measuring pore size values as

$$\overline{X} = \frac{1}{N}\sum_{i=1}^{N} x_i \quad (5)$$

and

$$s = \sqrt{\frac{1}{N}\sum_{i}^{N}(x_i - \overline{x})^2} \quad (6)$$

respectively, where N is the total number of pore size values measured from SEM images, x_i is the pore size value and $\overline{x}$ is the average pore size value.

3. Results and discussion

3.1. Space-holder dissolution, phase identification and chemical analysis

The space-holder was eliminated by soaking it in water prior to sintering Fig. 1 shows the relative mass loss after soaking with respect to space-holder particle size range for each one of the space-holder volume percentages. A value of 100% corresponds to mass loss equivalent to the total mass of the space-holder present

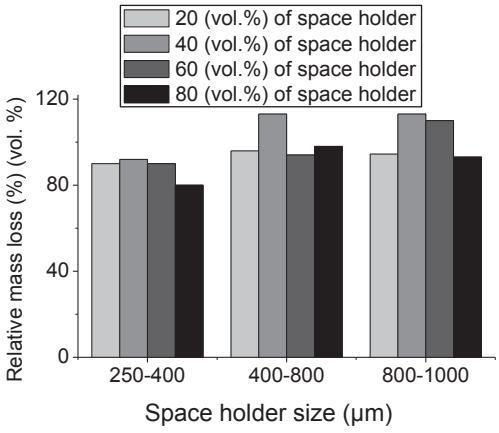

Fig. 1. Relative mass loss after soaking in water for different space-holder size distributions and volume percentages.

for each of the volume percentages and space-holder size ranges, respectively, hence corresponding to complete space-holder elimination. For smaller space-holder particle sizes the relative mass loss is slightly lower, indicating that it is probably more difficult to eliminate completely the smaller space-holder. Nevertheless the relative mass loss approaches values of around 90%, indicating that a relative small amount, if any, of space-holder remains after soaking. Increasing the amount of space-holder in the particle size range of 250–400 μm makes space-holder removal more difficult. However this is not observed for bigger particle size ranges, where no clear tendency of relative mass loss and volume percentage of space-holder is evident. For higher space-holder particle sizes the relative mass loss approaches values of almost 100% indicating almost complete space-holder removal. In some cases values above 100% are observed. Observations during this dissolution process suggest that this is probably due to loss of some MAX-phase powder itself, particularly in the case of higher space-holder particle size. Space-holder elimination is performed on the green body, before sintering and, although this is beneficial because it allows greater space-holder removal, on the other hand, at this stage, after cold pressing there is no diffusional bonding in-between particles therefore particle bonding is relatively weak, allowing for some powder loss during this dissolution process.

Fig. 2 shows the XRD spectrum plotted in terms of relative intensity for the raw powder, the sintered material without space-holder and two selected, but representative, samples of sintered foams. All samples have the same phases present: two major phases: Ti_2AlC and Ti_3AlC_2, and two minor phases, in small amounts: Al_2O_3 and TiC. The amount of the different phases present was determined by normalizing the intensity of the highest XRD peaks for each phase and is shown in Table 2. Similar phase composition for the starting Ti_2AlC powder, provided by this supplier, has been reported before [18]. It has also been reported that during sintering the amount of Ti_3AlC_2 phase increases and the amount of Ti_2AlC decreases, due to the decomposition of Ti_2AlC to Ti_3AlC_2 according to the following reaction [35].

$$2Ti_2AlC_{(s)} \rightarrow Ti_3AlC_{2(s)} + TiAl_{(1-x)} + xAl_{(g\ or\ l)} \quad (7)$$

where $x \leq 1$. Decompositon according to this reaction will be more severe in porous samples, as compared to fully dense samples, because of their high surface area, which allows faster loss of Al, due to its vaporization at high temperatures. Ti_3AlC_2 can also be formed by reaction of Ti_2AlC with TiC:

$$Ti_2AlC + TiC \rightarrow Ti_3AlC_2 \quad (8)$$

If decomposition of Ti_2AlC into Ti_3AlC occurs by reaction with TiC, the amount of decrease of Ti_2AlC should be similar to the amount of the increase of Ti_3AlC, whereas if decomposition occurs without reaction with TiC the amount of decrease of Ti_2AlC should be twice the amount of increase of Ti_3AlC. In the current study, for the sample without space-holder, the amount of decrease of Ti_2AlC is lower than the amount of increase of Ti_3AlC_2 and in addition the amount of TiC seems to decrease. A similar trend is observed for the foam with 20% of space-holder. Therefore decomposition is more likely to be occurring due to reaction with TiC in both cases. This suggests that the phase transformations occurring in the foam are similar to those that occur in the dense material and hence are not affected by any remaining amount of space-holder. For higher amount of space-holder (40 vol. %) it appears that the amount of Ti_2AlC actually increases. The exact mechanism by which this occurs it is not clear at present, however, this phase stabilization is considered beneficial.

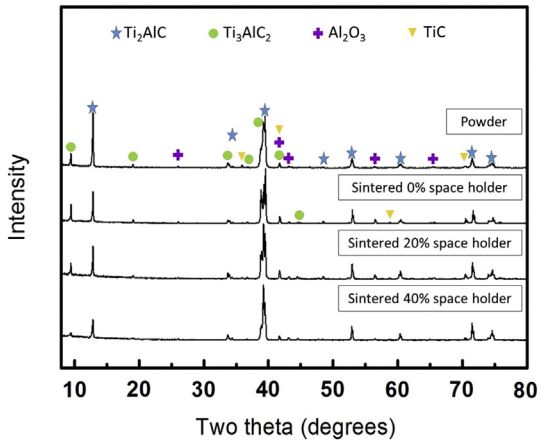

Fig. 2. XRD of starting Ti_2AlC powder, sintered material without space-holder and Ti_2AlC foams with 250–400 μm size distribution and different % in vol. of space-holder: 20% and 40%. The phase identification was performed using the Inorganic Crystal Structure Database (ICSD) collection code 165460 for Ti_2AlC, 153266 for Ti_3AlC_2, 10425 for Al_2O_3 and 44494 for TiC.

Table 2
Amount of the phases present in the starting Ti_2AlC powder, sintered Ti_2AlC sample and porous Ti_2AlC foams as determined by relative intensity of the highest peaks of each phase.

Sample	Amount of phases (%)			
	Ti_2AlC	Ti_3AlC_2	Al_2O_3	TiC
Starting Ti_2AlC Powder	67.9	25.0	4.3	2.9
Sample with 0 vol.% space-holder	61.0	37.2	1.2	0.6
Foam with 20 vol.% space-holder (250–400 μm)	63.7	32.5	2.5	1.3
Foam with 40 vol.% space-holder (250–400 μm)	75.8	21.2	1.5	1.5

The amount of retained sugar in the foams was also studied by chemical analysis of carbon content (Table 3). The powder used for making the foams contained 2% in weight of acrowax (used as pressing lubricant) and as a consequence contains 1.99 wt % more C than the raw starting powder. The sintered material without space-holder shows a lower amount of C than the starting powder with acrowax due to the fact that the acrowax lubricant is burned at sintering cycle during the 30 min dwell step at 400 °C, so after sintering the % wt. of C decreases. However, the amount of C for sintered material without space-holder is still higher than the raw starting powder. This is attributed to mass loss during sintering, specifically to loss of Al, even possibly some Ti, that can both vaporize at high temperature and escape from the sample. A mass loss of around 5 wt.% was measured after sintering for the materials without space-holder, and higher amounts up to 8 wt% was observed for porous samples that show higher mass loss due to higher surface area. Reports of mass loss for this type of material during sintering have been previously reported [18]. Sintered foams exhibit values close to sintered material without space-holder and to the theoretical content in Ti_2AlC and variations of carbon contents in foams after dissolution are low. Therefore it can be concluded that overall the dissolution process is successful, no additional C is introduced due to the presence of the space-holder and phase transformations occurring in the foams are similar to those that would occur in the starting powder due to sintering.

3.2. Characterization of porosity, pore morphology and foam microstructure

Porosity was quantitatively characterized by determination of open, closed and total porosity. Fig. 3 shows the variation of porosity with the volume percentage of space-holder for different sizes of space-holder. All the foam samples were compared to the

Table 3
Chemical analysis of carbon content in starting powder, sintered sample without space-holder and sintered foams with space-holder particle size distribution of 800–1000 μm and different volume of space-holder. The theoretical value in powder was calculated as the theoretical % wt. C contained in stoichiometric Ti_2AlC.

% Wt C							
Theoretical content in Ti2AlC	Powder		Sintered foams				
	Starting powder	Powder + 2% acrowax	Volume percentage of space-holder (size range 800–1000 μm)				
			0%	20% vol.	40% vol.	60% vol.	80% vol.
8.91	7.86	9.85	8.42	9.09	9.62	9.60	9.58

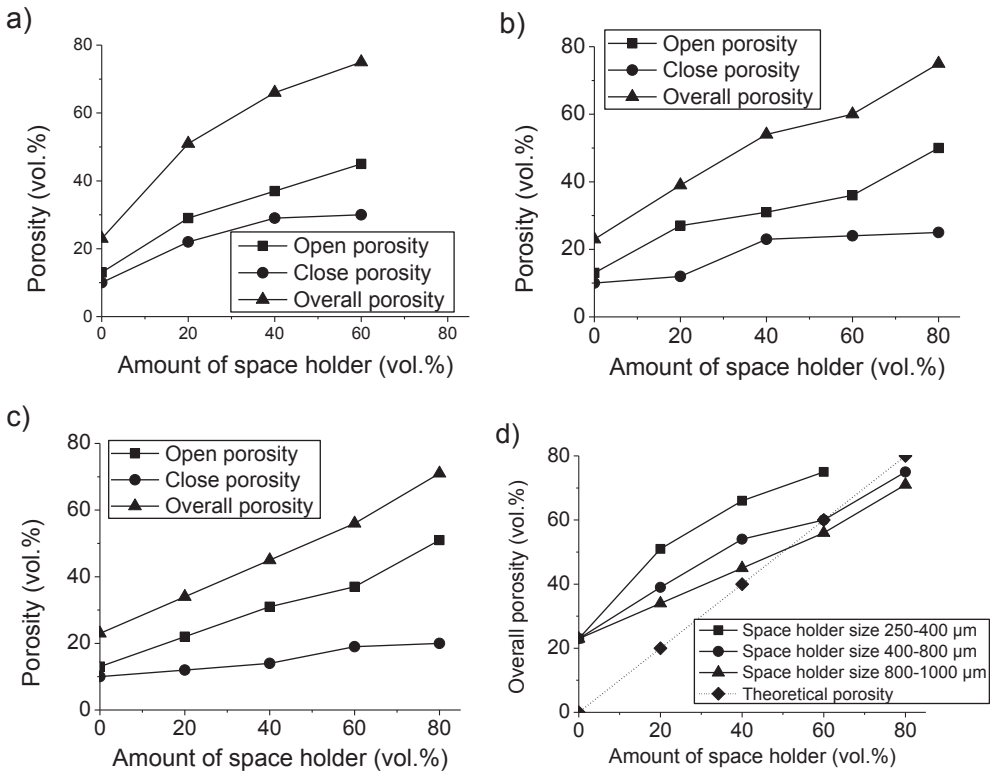

Fig. 3. Variation of porosity with the amount of space-holder added for different space-holder size distributions (a) 250–400 μm, (b) 400–800 μm and (c) 800–1000 μm. (d) Overall porosity variation with space-holder percentage for different space-holder sizes. The dotted line indicates the theoretical porosity that the foam would have if all its porosity due to the space-holder.

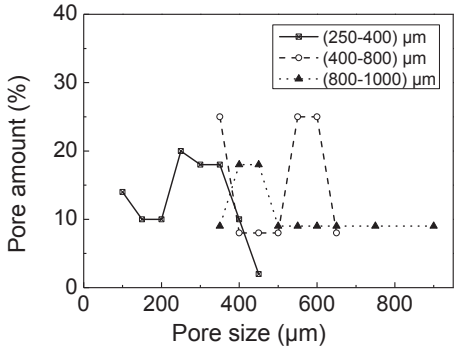

Fig. 4. Pore amount (%) versus pore size for three pore size ranges (250–400 μm, 400–800 μm, 800–1000 μm) and fixed space-holder amount (60 vol.%).

sintered material without space-holder which was pressed and sintered under the same conditions as the foams. For all foams most of the porosity appears to be open porosity (interconnected). Closed porosity remains relatively stable with the increase in space-holder volume percentage, and this effect is emphasized with the increase in the size of space-holder. On the contrary, open porosity increases with space-holder volume percentage, regardless of space-holder size. Therefore it appears that most of the porosity due to the addition of space-holders is open interconnected porosity. Closed porosity may be due to an incomplete densification during sintering.

Porosity obtained experimentally does not match the theoretical expected porosity due to amount of space-holder added (Fig. 3d). The overall porosity percentage is higher than the theoretial expected porosity up to 40% volume of space-holder added. This confirms that part of the porosity present is also partially a result of incomplete sintering. From 40% up to 80% vol. space-holder, overall porosity is lower than theoretical porosity. During the elimination

Table 4
Comparison between average pore size measured by image analysis and space-holder size for three size ranges. Space-holder average size, D_{50}, corresponds to the average size measured with particle size analysis. The space-holder average size after shrinkage corresponds to the average size of the space-holder minus the shrinkage (%) experimentally measured for each space-holder size range.

Average pore size (μm)	Space-holder range (μm)	Space-holder average size D_{50} (μm)	Space-holder average size after shrinkage (μm)
229 ± 97	250–400	385	368
478 ± 157	400–800	640	609
513 ± 166	800–1000	1015	962

of the space-holder mass loss occurred due to the dissolution of the space-holder as well as removal of some powder, as already mentioned. This could lead to a modification in the structure decreasing the overall porosity.

Porosity was also characterized by image analysis on foams with 60% vol. of space-holder with three size distributions: 250–400 μm, 400–800 μm and 800–1000 μm (Fig. 4). The range of particle size distribution measured from image analysis is in agreement with the particle size for smaller space-holder particle sizes (250–400 μm). For the intermediate (400–800 μm) space-holder size distribution it appears that most of the pores (about 60%) are above 500 μm in size, whereas there is also a considerable percentage of pores (about 25%) with sizes smaller than 400 μm. Similarly, for the biggest space-holder size distribution (800–1000 μm) there is a constant distribution of pore sizes above about 500 μm, however there is a considerable percentage of pores with sizes smaller than 500 μm, outside the range of the space-holder initial size.

The average pore size and standard deviation obtained from image analysis is presented on Table 4. The particle size measured by image analysis is compared to the average space-holder size for each one of the space-holder size ranges. The average space-holder

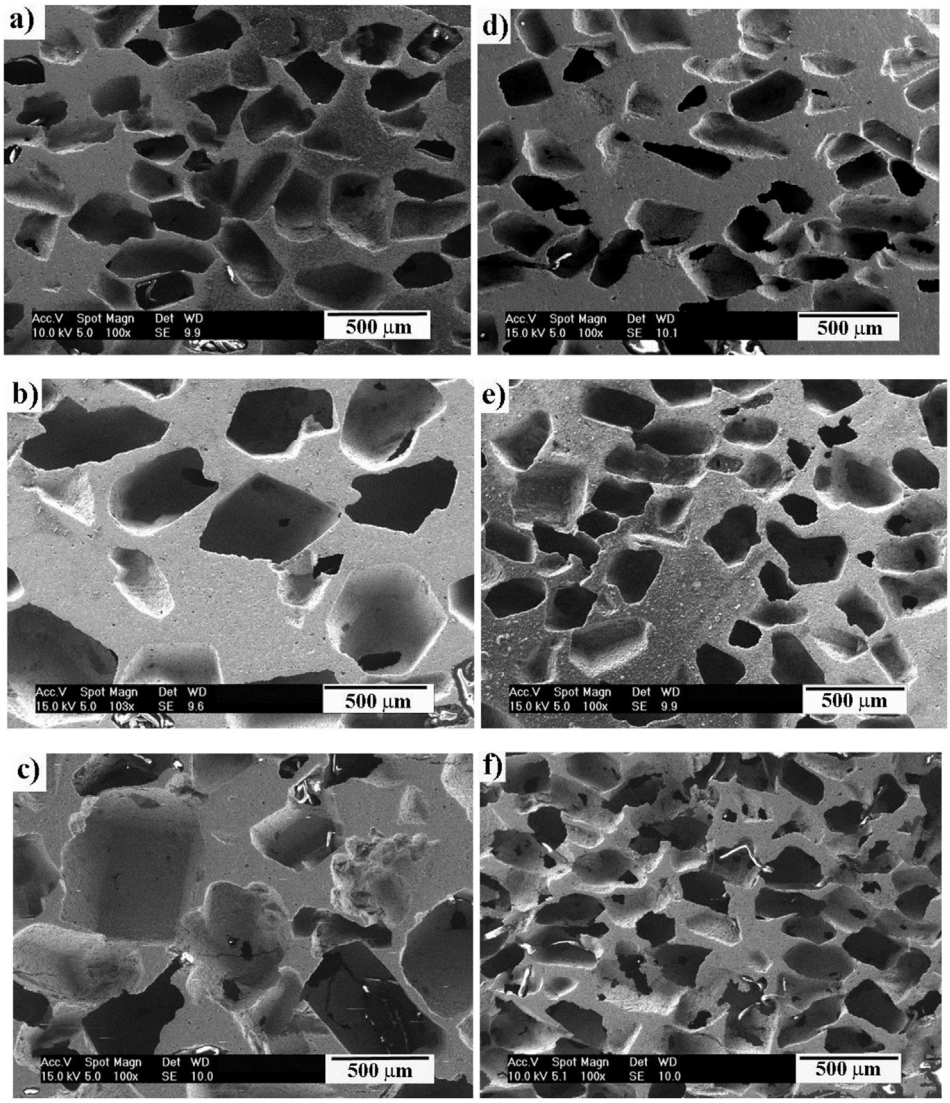

Fig. 5. Secondary electron microcopy image of a Ti_2AlC foams. With 60% volume percentage of space-holder for three space-holder size distributions: (a) 250–400 μm, (b) 400–800 μm, (c)800–1000 μm. With 250–400 μm space-holder size distribution for three volume space-holder percentages: (d) 20%, (e) 40% and (f) 80%.

size for each one of the space-holder size ranges was measured prior to foam production (Table 1). However, during sintering some shrinkage occurs which will modify the expected pore size. The expected average space-holder pore size considering the shrinkage observed experimentally during sintering is also presented in Table 4. For this calculation it was assumed that shrinkage occurs homogeneously. For all space-holder particle size ranges the measured average pore size is smaller than the expected pore size due to space-holder size, even after considering the shrinkage. This is especially the case for larger space-holder size range (800–1000 μm), where there are also a considerable number of pores with sizes outside the range of the initial space-holder size, which could be a result of collapsing of bigger pores. These results indicate final average pore size will, in general, be smaller than the initial space-holder size, especially for larger space-holder size. This is probably both due to shrinkage during sintering as well as bigger pores splitting into smaller ones.

Fig. 5 shows SEM images of the foams obtained for different space-holder sizes and volume percentages. Pore morphology is not directional and pores are relatively homogeneous and randomly distributed. When volume percentage of space-holder increases, the percentage of porosity and homogeneity in porosity increases. If the space-holder amount increases, the possibility of space-holder particles touching increases producing interconnected pores. Previous studies with leachable space-holders show that with increasing amount of space-holder, pores become more elliptical and oriented as a consequence of crushing during cold pressing [18]. It is worth nothing that this effect is not observed in this case, even for 80% volume of space-holder.

The microstructure of the foams was examined in more detail using backscatter electron microscopy and EDX. Fig. 6 shows a representative image of microstructure of the necks, or dense regions, in between the pores at high magnification. Two phases can be observed: 1) a main matrix phase with darker color and 2) another minor phase with a lighter color. In addition, microporosity is clearly visible in this region, confirming the porosity measurement results that indicated a large amount of closed porosity is present due to incomplete sintering. Table 5 shows the results of the EDX analysis realized on the two phases observed. The stoichiometric relationship between Ti, Al and C on the main matrix phase confirms that this corresponds to the Ti_2AlC, as detected by XRD, whereas the light phase most probably corresponds to Ti_3AlC_2. The minor phases, Al_2O_3, and TiC, detected by XRD were not observed by EDX, neither on the foams nor in the material without space-holder. It is possible that the light phase, or part of it, might also correspond to TiC phase, since the difference in contrast between TiC and Ti_3AlC_2 in the backscattered electron image might not be sufficient to differentiate between them. In addition, this phase is considerably narrower than the matrix, so the EDX analysis is less accurate, taking information from the elements contained in neighboring area (Ti_2AlC). These results are in agreement with the XRD phase identification. In general the microstructure of the obtained foams is consistent with the expected for this material.

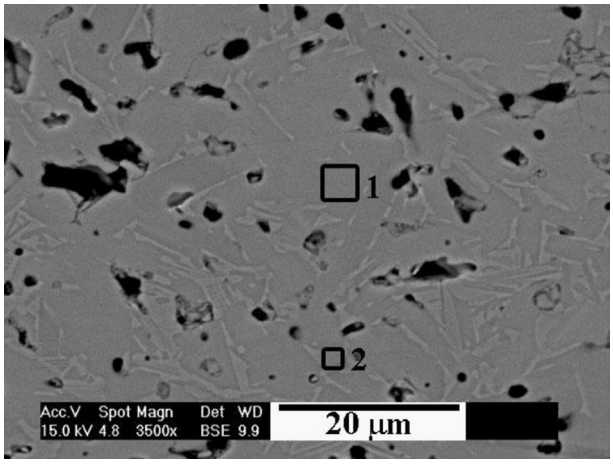

Fig. 6. Secondary electron image (Backscattered mode) of foam with 60% volume percentage and space-holder size distribution of 800–1000 μm. Two phases are distinguished: 1) matrix phase (darker area) and 2) secondary phase (lighter area).

Table 5
EDX analysis of sintered sample without space-holder and sintered foams with different the same space-holder size distributions and volume percentages.

Sample	Dark area (at %) (1)			Light area (at %) (2)		
	Ti	Al	C	Ti	Al	C
Without space-holder	48	24	28	51	17	32
20%vol. (250-400) μm space-holder	53	23	24	57	27	16
40%vol. (250-400) μm space-holder	51	26	23	60	7	33
60%vol. (250-400) μm space-holder	51	27	22	58	11	31
80%vol. (250-400) μm space-holder	51	27	22	55	7	38
60%vol. (400-800) μm space-holder	56	29	15	60	6	34
60%vol. (800-1000) μm space-holder	51	27	22	67	1	32

4. Conclusions

A simple, economic and environmentally friendly process was employed to make porous Ti_2AlC foams employing raw sugar as space-holder with controlled porosity amount and size. Mass loss measurement after space-holder dissolution, C chemical analysis and phase identification confirm successful removal of leachable space-holder. The overall, open and closed porosity and distribution was characterized. Foams with homogenous porosity ranging from 23 vol% to 76 vol% where successfully produced. Differences were found between experimental and expected porosity. For space-holder addition lower than 40% in volume, experimental porosity is higher than expected and the opposite occurs for space-holder additions higher than 40%. Differences between expected and experimental porosity are due to a combined effect of incomplete sintering and material loss during space-holder dissolution. Average pore size in the produced foams is in general smaller than the initial space-holder size, as a result of sintering, and this is more pronounced for bigger space-holder sizes. Phase evolution during sintering shows partial decomposition of Ti_2AlC into Ti_3AlC_2.

Acknowledgments

The authors wish to thank the Ministry of Education and Science for funding through R & D project MAT2012-38650-C02-01, and the Community of Madrid for its funding through ESTRUMAT program (S-2009/MAT-1585).

References

[1] M.W. Barsoum, The $M_{(N+1)}AX_{(N)}$ phases: A new class of solids; thermodynamically stable nanolaminates, Prog. Solid State Chem. 28 (2000) 201–281.
[2] Z.M. Sun, Progress in research and development on MAX phases: a family of layered ternary compounds, Int. Mater. Rev. 56 (2011) 143–166.
[3] M. Radovic, M.W. Barsoum, MAX phases: bridging the gap between metals and ceramics, Am. Ceram. Soc. Bull. 92 (2013) 20–27.
[4] X.H. Wang, Y.C. Zhou, Microstructure and properties of Ti_3AlC_2 prepared by the solid-liquid reaction synthesis and simultaneous in-situ hot pressing process, Acta Mater. 50 (2002) 3141–3149.
[5] X.H. Wang, Y.C. Zhou, Oxidation behavior of Ti_3AlC_2 at 1000–1400 degrees C in air, Corros. Sci. 45 (2003) 891–907.

[6] X.H. Wang, Y.C. Zhou, High-temperature oxidation behavior of Ti_2AlC in air, Oxid. Metals 59 (2003) 303–320.
[7] X.H. Wang, Y.C. Zhou, Layered machinable and electrically conductive Ti_2AlC and Ti_3AlC_2 ceramics: a review, J. Mater. Sci. Technol. 26 (2010) 385–416.
[8] S. Basu, N. Obando, A. Gowdy, I. Karaman, M. Radovic, Long-term oxidation of Ti_2AlC in air and water vapor at 1000–1300 degrees C temperature range (vol 159, pg C90, 2012), J. Electrochem. Soc. 159 (2012). S9-S.
[9] J.W. Byeon, J. Liu, M. Hopkins, W. Fischer, N. Garimella, K.B. Park, et al., Microstructure and residual stress of alumina scale formed on Ti2AlC at high temperature in air, Oxid. Metals 68 (2007) 97–111.
[10] M.W. Barsoum, I. Salama, T. El-Raghy, J. Golczewski, W.D. Porter, H. Wang, et al., Thermal and electrical properties of Nb_2AlC, $(Ti, Nb)_2AlC$ and Ti_2AlC, Metall. Mater. Trans. A-Phys. Metall. Mater. Sci. 33 (2002) 2775–2779.
[11] N.P. Brodnikovskii, M.P. Burka, D.G. Verbilo, A.N. Demidik, I.I. Ivanova, A.Y. Koval, et al., Structure and mechanical properties of porous titanosilicon carbide Ti_3SiC_2, Powder Metall. Metal Ceram. 42 (2003) 424–432.
[12] S.A. Firstov, V.F. Gorban, I.I. Ivanova, E.P. Pechkovskii, Mechanical properties of porous Ti_3SiC_2/TiC, Ti_3AlC_2/TiC, and Ti_4AlN_3/TiN Nnanolaminates at 20 to 1300 degrees C, Powder Metall. Metal Ceram. 49 (2010) 414–423.
[13] S.A. Firstov, E.P. Pechkovskii, I.I. Ivanova, N.P. Brodnikovskii, V.F. Gorban, A.N. Demidik, Effect of the composition and porosity of sintered titanium nanolaminates on their mechanical properties at high temperatures, Strength Mater. 38 (2006) 624–636.
[14] M. Fraczkiewicz, A.G. Zhou, M.W. Barsoum, Mechanical damping in porous Ti_3SiC_2, Acta Mater. 54 (2006) 5261–5270.
[15] Z.M. Sun, A. Murugaiah, T. Zhen, A. Zhou, M.W. Barsoum, Microstructure and mechanical properties of porous Ti_3SiC_2, Acta Mater. 53 (2005) 4359–4366.
[16] A.G. Zhou, M.W. Barsoum, S. Basu, S.R. Kalidindi, T. El-Raghy, Incipient and regular kink bands in fully dense and 10 vol.% porous Ti_2AlC, Acta Mater. 54 (2006) 1631–1639.
[17] A.G. Zhou, M. Fraczkiewicz, M.W. Barsoum, Mechanical damping in porous Ti_3SiC_2, Acta Mater. 54 (2006) 5261–5270.
[18] L. Hu, R. Benitez, S. Basu, I. Karaman, M. Radovic, Processing and characterization of porous Ti_2AlC with controlled porosity and pore size, Acta Mater. 60 (2012) 6266–6277.
[19] L. Hu, I. Karaman, M. Radovic, Simple, inexpensive synthesis of damage-tolerant MAX phase foams, Am. Ceram. Soc. Bull. 92 (2013) 31–32.
[20] S. Amini, C. Ni, M.W. Barsoum, Processing, microstructural characterization and mechanical properties of a $T_{i2}AlC$/nanocrystalline Mg-matrix composite, Compos. Sci. Technol. 69 (2009) 414–420.
[21] S. Amini, M.W. Barsoum, On the effect of texture on the mechanical and damping properties of nanocrystalline Mg-matrix composites reinforced with MAX phases, Mater. Sci. Eng. A-Struct. Mater. Prop. Microstruct. Process. 527 (2010) 3707–3718.
[22] A. Kontsos, T. Loutas, V. Kostopoulos, K. Hazeli, B. Anasori, M.W. Barsoum, Nanocrystalline Mg-MAX composites: mechanical behavior characterization via acoustic emission monitoring, Acta Mater. 59 (2011) 5716–5727.
[23] Z. Sun, Y. Lang, M. Li, Y. Zhou, Preparation of reticulated MAX-phase support with morphology-controllable nanostructured ceria coating for gas exhaust catalyst devices, J. Am. Ceram. Soc. 93 (2010) 2591.
[24] A. Kennedy, in: Katsuyoshi Kondoh (Ed.), Porous Metals and Metal Foams Made from Powders, Powder Metallurgy, 2012, ISBN 978-953-51-0071-3 (InTech).
[25] P. Fernández, L.J.J. Cruz, J. Coleto, Manufacturing processes of cellular metals. Part II. Solid route, metals deposition, other processes, Rev. Metal. 45 (2) (2009) 124–142.
[26] N. Michailidis, F. Stergioudi, D. Tsipas, Manufacturing of open-cell metal foams using a novel leachable pattern, Adv. Eng. Mater. 13 (2011) 29–32.
[27] F. Stergioudi, G. Karelis, E. Paulidou, N. Michailidis, Production and structural characterization of tailored made open-cell alumina-vanadia foams, Ceram. Int. 39 (2013) 8065–8072.
[28] N. Michailidis, F. Stergioudi, A. Tsouknidas, Deformation and energy absorption properties of powder-metallurgy produced Al foams, Mater. Sci. Eng. A A 528 (2011) 7222–7227.
[29] Seksak Asavavisithchai, Ekasit Nisaratanaporn, Fabrication of open-cell silver foams using disaccharide as space holders, Chiang Mai J. Sci. 37 (2) (2010), 222–30. 25.
[30] G. Adamek, D. Andrzejewski, J. Jakubowicz, Sugar crystals as a space holder material for Ti void metal composites, J. Biomater Tissue Eng. 4 (2014) 300–307.
[31] J. Jakubowicz, G. Adamek, M. Dewidar, Titanium foam made with saccharose as a space holder, J. Porous Mater. 20 (2013) 1127–1141.
[32] J.B. Mao, F.L. Zhang, G.C. Liao, Y.M. Zhou, H.P. Huang, C.Y. Wang, S.H. Wu, Effect of granulated sugar as pore former on the microstructure and mechanical properties of the vitrified bond cubic boron nitride grinding wheels, Mater. Des. 60 (2014) 328–333.
[33] Y.Y. Zhao, D.X. Sun, A novel sintering-dissolution process for manufacturing Al foams, Scr. Mater. 44 (2001) 105–110.
[34] S. Ziqi, L. Ying, L. Meishuan, Z. Yanchun, Preparation of reticulated MAX-phase support with morphology-controllable nanostructured ceria coating for gas exhaust catalyst devices, J. Am. Ceram. Soc. 93 (9) (2010) 2591–2597.
[35] Cb Spencer, J.M. Cordona, N. Obando, A. Sakulich, R. Miladin, M. Odem, L. Hultma, L.W. Barsoum, Phase evaluation in $A_{l2}O_3$ fiber-reinforced Ti_2AlC during sintering in the 1300 degrees C-1500 degrees C temperature range, J. Am. Ceram. Soc. 94 (2011) 3327–3334.

B. Velasco, E. Gordo, S.A. Tsipas*
Departamento de Ciencia e Ingeniería de Materiales e Ingeniería Química, IAAB, Universidad Carlos III de Madrid, Avda. de la Universidad, 30, 28911, Leganés, Madrid, Spain

* Corresponding author.
E-mail address: stsipas@ing.uc3m.es (S.A. Tsipas).

27 October 2014
Available online 20 June 2015